International Journal of Fluid Power 10 (2009) No. 1 pp. 17-25

APPLICATION OF EXTENDED KALMAN FILTER IN A METERING POPPET VALVE SYSTEM

Chang Li and Roger Fales

Rolf Fluid Power Lab, Mechanical and Aerospace Engineering University of Missouri-Columbia Columbia, Missouri 65211
clbk6@mizzou.edu, FalesR@missouri.edu

Abstract

This work focuses on an accurate Extended Kalman Filter (EKF) estimator, which is applied to a forced-feedback metering poppet valve system (FFMPVS). The EKF estimator is used to estimate the position and velocity of the main poppet valve, position and velocity of the pilot poppet valve and pressures within the pilot stage of the valve. The EKF estimator takes advantage of its recursive optimal state estimation to estimate the states of this metering poppet valve by using one pressure signal measurement. The results from the EKF are compared with the simulation results from the model and also compared with the states which can be measured from the physical system set up in the lab. It is shown that the EKF estimator tracks the states accurately for both the steady-state and transient performance. The EKF estimator has robustness to parameter variations. It is shown specifically that the EKF estimator has robustness to an example of model uncertainty, variations in the spring stiffness parameter.

Keywords: Extended Kalman Filter, metering poppet valve, robustness

1 Introduction

The metering poppet valve discussed in this paper is a unique design developed at the University of Missouri with two stages: a pilot stage and a main stage. Both stages employ poppet valves rather than more common spool valves. Previous work focused on the experimental evaluation of the valve, which is studied by Fales and Li (2008). Experiments were carried out to correct the model parameters based on the actual construction of the valve. The parameters in the simulation were adjusted to match experimental results since there were some dynamic characteristics of the model such as friction that require experimental data to determine. The dynamic response was analyzed by comparing the experimental results with the nonlinear and linear model simulations. The system response is found to have very high speed. The performance varies based on changes in operating conditions and model uncertainty.

From the results of previous work, it is found that in the metering poppet valve model, there are several sources of model uncertainties. (a) Parameters can vary from valve to valve if the valve were to be mass produced or as the valve wears over time causing model uncertainty. (b) The complexity of the geometry makes the determination of a physics based flow force model difficult. (c) The model linearization changes depending on operating conditions which can also be treated as uncertainty. Another problem is that the measurement of the control volume pressure is disturbed by sensor noise. A common solution to the noise problem is to introduce low pass filtering, but the filtering will also restrict the transient performance of the pressures, which have very high speed dynamics.

In order to obtain higher performance, the metering poppet valve system needs the position of the main poppet and the pilot poppet as the feedback signals for the close loop controller. Also, the system needs the pressure measurements for pressure control. Measuring the position of the main poppet or the pilot poppet directly by using the Linear Variable Differential Transformer (LVDT) is possible, but it is impossible to measure the positions of the two poppets simultaneously because of the physical limitations of the system. In order to obtain the positions and pressures of the system, an estimator is necessary.

This newly developed forced-feedback metering poppet valve system is a nonlinear and multiple input and output system, which has a lot of model uncertain-

This manuscript was received on 14 October 2008 and was accepted after revision for publication on 22 January 2009

ties. In the very limited existing literature, a linear observer is discussed by Muller and Fales (2008). Although the linear observer tracks the steady state response of the system well, it cannot follow the transient response closely and it is fragile to system nonlinearity, parameter variation, operating conditions changes and other model uncertainties. Also, it requires highly precise measurement for estimating, which increases the cost for high performance sensors.

The EKF estimator is one of the most widely used solutions for determining unmeasured signals in dynamic systems. It has been applied to many different kinds of systems and works well for many systems. The application of the EKF in fault detection in hydraulically actuated systems is described in detail by An and Sepehri (2005); the EKF for the direct torque controlled interior permanent magnet synchronous motor drive is discussed by Zhuang Xu and M. F. Rahman (2003); using the EKF to develop a sliding mode control system for subjugator by Walchko, Novick and Nechyba. (2003). An EKF was shown to be able to estimate bulk modulus and viscous damping coefficients in a high performance electro hydraulic actuator by Chinniah, Burton and Habibi. (2003). All these examples show that the EKF is suitable for tracking and filtering due to its optimality, tractability and robustness to model uncertainties for nonlinear systems. Therefore, the EKF estimator is suitable for this metering poppet valve system due to its accurate estimations and robustness to model uncertainties.

2 Dynamic Model of the Metering Poppet Valve System

The metering poppet valve model is briefly discussed in this section. More details can be found in previous works by Muller and Fales (2008). A description of the operation of the valve design is presented in the work by the Fales and Li (2008).

System dynamics are based on the metering poppet valve system shown in Fig. 1.

The actuator force applied to the pilot poppet, F, is the only input to the system while the dynamic variables are the pilot poppet position, x, the pilot poppet velocity, $\dot{x}$, the main poppet position, y, the main poppet velocity, $\dot{y}$, the control volume pressure between the main and pilot poppet, P_C, and the control volume pressure between the pilot poppet and the actuator housing, P_P. The state vector is chosen to be $\boldsymbol{x} = [x\ \dot{x}\ y\ \dot{y}\ P_C\ P_P]^T$ with measured output, $\boldsymbol{y} = [P_C]$, and input, $\boldsymbol{u} = [F]$.

The control volume pressure between the main and pilot poppet, P_C, is chosen as the output because it can be easily measured by using a pressure sensor and the system is observable with the corresponding output matrix. The nonlinear valve system equations are represented by Eq. 1 to Eq. 4, which are discussed in detail by Muller and Fales (2008).

$$\ddot{x} = \frac{1}{m}\left[-k\left(x + y + preload\right) - b_x\dot{x} - A_{pilot}\left(P_C - P_P\right) + f_1 - f_2 + F\right] \quad (1)$$

$$\ddot{y} = \frac{1}{M}\left[-k\left(x + y + preload\right) - b_y\dot{y} - A_C P_C + A_L P_L + A_S P_S - f_3\right] \quad (2)$$

$$\dot{P}_C = \beta\frac{Q_1 - Q_2 - Q_6 + A_C\dot{y}}{V_C 0 - A_{pilot}x - A_C y} \quad (3)$$

$$\dot{P}_P = \beta\frac{Q_6 - A_{pilot}\dot{x}}{V_{pilot}0 + A_{pilot}x} \quad (4)$$

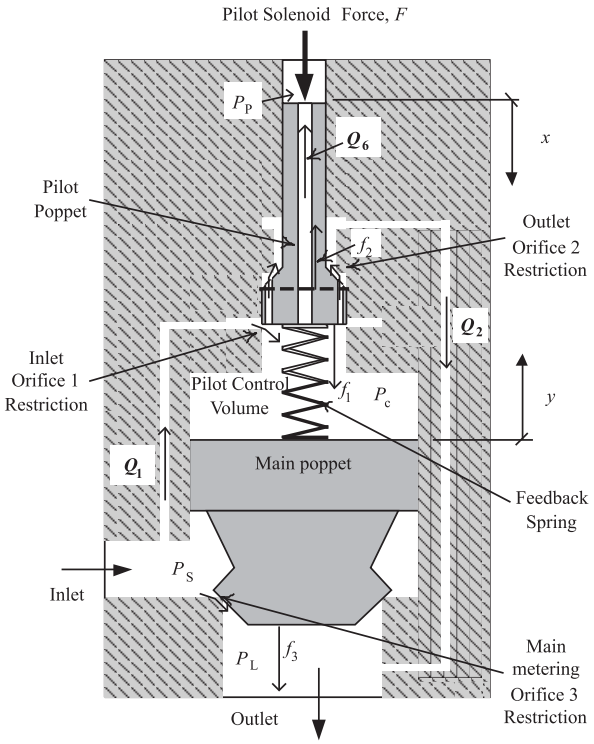

Fig 1: *Metering poppet valve with a forced-feedback configuration*

In Eq. 2, P_S is the supply pressure and P_L is the load pressure through the return line. In the simulation, the data measured for these two pressures from the experiment is used to supply the value for each of them. The terms, f_1 and f_2, represent the flow forces on the pilot poppet while f_3 represents the flow force on the main poppet (See Fig. 1). The steady state flow forces are shown in Eq. 5 to 7. Though transient flow forces may have some effect on the system dynamics, the flow forces considered in this work neglect any transient terms. Neglecting the transient flow forces represents a simplification of the model which the authors feel is justified since these terms are likely small.

$$f_1 = 2\cos(\theta)C_d^2\left(h_1 x + a_{1\max}\right)\left(P_S - P_C\right) \quad (5)$$

$$f_2 = 2\cos(\theta)C_d^2 h_2 x\left(P_C - P_L\right) \quad (6)$$

$$f_3 = 2\cos(\theta)C_d^2 h_3 y\left(P_s - P_L\right) \quad (7)$$

Q_1 is the flow rate across the inlet orifice to control volume. Q_2 is the flow rate across the outlet orifice from control volume. The flows are modeled using the standard orifice equation as shown in Eq. 8 and Eq. 9.

$$Q_1 = C_d\left(h_1 x + a_{1\max}\right)\sqrt{\frac{2}{\rho}\left(P_S - P_C\right)} \quad (8)$$

$$Q_2 = C_d h_2 x \sqrt{\frac{2}{\rho}\left(P_C - P_L\right)} \tag{9}$$

Q_6 is the low Re tube flow through a circular tube in the pilot poppet which connects P_C to P_P and is modeled using Eq. 10.

$$Q_6 = \frac{\pi R^4}{8\mu L_{\text{pilot}}}(P_C - P_P) \tag{10}$$

The flow through the tube, Q_6, creates a viscous damping effect on the pilot poppet by creating pressure difference between P_C and P_P which leads to a force imbalance on the pilot poppet when motion causes flow through the tube. In Eq. 2, the viscous friction terms, b_x and b_y, were determined by comparing experimental responses to simulations and adjusting the parameters as needed. These friction coefficients would be difficult to determine accurately by analytical means due to the many factors involved. Further work to experimentally determine the friction characteristics under a wide variety of conditions could be used to improve the accuracy of the friction model but was not pursued in this work. A nonlinear friction model would also improve accuracy, though steps were taken to minimize the effects of nonlinear friction as described in Section 4. The viscous friction force on the main poppet is small compared to the hydrostatic forces and was found to have a small effect on simulation responses under the conditions seen in lab experiments. The viscous friction force on the pilot poppet had a more significant effect on simulations but was smaller than damping effect caused by the flow, Q_6.

All remaining parameters which appear in Eq. 1 through Eq. 10 are constants as shown in the Nomenclature section.

The EKF estimator requires the state space model of the system, which is obtained by linearizing the model equations with respect to the state vector at each time step. Online computation of state space matrix (Jacobian matrix) is shown in Eq. 11,

$$\mathbf{A}_k = \left.\frac{\partial \mathbf{F}(\boldsymbol{x},\boldsymbol{u},t)}{\partial \boldsymbol{x}}\right|_{\boldsymbol{x}=\hat{\boldsymbol{x}}_k} = \begin{bmatrix} 0 & 1 & 0 & 0 & 0 & 0 \\ f_{21} & f_{22} & f_{23} & 0 & f_{25} & f_{26} \\ 0 & 0 & 0 & 1 & 0 & 0 \\ f_{41} & 0 & f_{43} & f_{44} & f_{45} & 0 \\ f_{51} & 0 & f_{53} & f_{54} & f_{55} & f_{56} \\ f_{61} & f_{62} & 0 & 0 & f_{65} & f_{66} \end{bmatrix}_{\boldsymbol{x}=\hat{\boldsymbol{x}}_k} \tag{11}$$

where $\mathbf{F}(\boldsymbol{x},\boldsymbol{u},t) = \frac{d}{dt}\begin{bmatrix} x & \dot{x} & y & \dot{y} & P_C & P_P \end{bmatrix}^T$.

The detailed calculation of the elements of Jacobian matrix is shown in part I of the Appendix.

Before attempting to implement the EKF estimator for the metering poppet valve system for estimating states, it is necessary to examine the observability of the system. The system must be observable to successfully implement the EKF in a way that will result in accurate state estimates. The EKF estimator uses measured pressure, P_C, to determine the state estimates. Therefore, the output matrix, C, of the system is

$$\mathbf{C} = [0\ \ 0\ \ 0\ \ 0\ \ 1\ \ 0].$$

Fortunately the observability matrix ,

$$[\mathbf{C}\ \ \mathbf{CA}\ \ \mathbf{CA}^2\ \ \mathbf{CA}^3\ \ \mathbf{CA}^4\ \ \mathbf{CA}^5]^T,$$

formed using the **A** and **C** matrices at a nominal operating point is full rank. This means that for a particular linearization at a steady state operating condition, the system is observable. While not every possible operating condition has been checked, this gives some confidence to move forward with estimator design since the system is found to be observable at the nominal operating conditions.

3 Extended Kalman Filter

The EKF has two main advantages in that it: (1) can provide optimal estimation of states for a nonlinear system under changing operating conditions, and (2) provides a solution for estimating states when there are model uncertainties and measurement noise.

The EKF estimator uses a two-step recursive algorithm for estimating and filtering. At the given sampling time t_k, both the priori optimal estimate states $\hat{\boldsymbol{x}}_k^-$ and the error covariance matrix $\mathbf{P}_k^-$ go into the EKF loop. The over-hat (^) indicates the variable is an estimate, and the superscript (-) denotes the best estimate before correcting for the current state measurement. An initial guess of $\hat{\boldsymbol{x}}_k^-$ and $\mathbf{P}_k^-$ is necessary to start the Kalman Filter Loop.

The first step for the EKF estimator is to compute the optimal state estimations. It includes three procedures: (1) calculate the Kalman gain used for this sampling time, (2) calculate the optimal state estimations, $\hat{\boldsymbol{x}}_k$ at t_k by updating the measurement through the measured pressure, P_C at t_k, and (3) update the error covariance matrix. These procedures are shown in Eq. 12 to 14.

$$\mathbf{K}_k = \mathbf{P}_k^- \mathbf{C}_k^T \left(\mathbf{C}_k \mathbf{P}_k^- \mathbf{C}_k^T + \mathbf{W}_k\right)^{-1} \tag{12}$$

$$\hat{\boldsymbol{x}}_k = \hat{\boldsymbol{x}}_k^- + \mathbf{K}_k\left(\boldsymbol{y}_k - \mathbf{C}_k \hat{\boldsymbol{x}}_k^-\right) \tag{13}$$

$$\mathbf{P}_k = \left(\mathbf{I} - \mathbf{K}_k \mathbf{C}_k\right)\mathbf{P}_k^- \tag{14}$$

where $\mathbf{C}_k$ is the output matrix. $\mathbf{W}_k$ is the measurement noise variance matrix, which is a zero-mean stochastic process determined by sensor specifications. It is a diagonal matrix containing the variances (σ^2) of the sensors. $\boldsymbol{y}_k$ is the new measurement, P_C, at t_k. The measurement noise matrix is of dimension 1 × 1 since P_C is the only measurement for the implementation of EKF.

The second step of the EKF loop is to project the state estimations and the error covariance matrix ahead in time for next loop. A modified second-order Euler integration technique is applied based on the system inputs, $\boldsymbol{u}_k$, at t_k when projecting the state estimations as shown in Eq. 15 and Eq. 16.

$$\boldsymbol{x}_{k+1}^* = \hat{\boldsymbol{x}}_k + T_s \mathbf{F}\left[\hat{\boldsymbol{x}}_k, \boldsymbol{u}_k\right] \tag{15}$$

$$\boldsymbol{x}_{k+1}^{-} = \frac{1}{2}\left(\hat{\boldsymbol{x}}_k + \boldsymbol{x}_{k+1}^{*} + T_s \mathbf{F}\left[\boldsymbol{x}_{k+1}^{*}, \boldsymbol{u}_k\right]\right) \quad (16)$$

The error covariance matrix is projected ahead as shown in Eq. 17 by updating the discrete state transition matrix (STM), $\mathbf{\Phi}_k$, which is the discrete Jacobian matrix of the nonlinear state equations.

$$\mathbf{P}_{k+1}^{-} = \mathbf{\Phi}_k \mathbf{P}_k \mathbf{\Phi}_k^{T} \quad (17)$$

$\mathbf{\Phi}_k$ is updated by computing the linearized state space matrix, A_k, evaluated at t_k as shown in Eq. (18).

$$\mathbf{\Phi}_k = \mathbf{I} + \mathbf{A}_k T_s + \frac{1}{2}\mathbf{A}_k^{\,2} T_s^{2} \quad (18)$$

T_s is the sampling period.

Figure 2 shows the complete EKF loop, which forms a recursive loop providing an optimal state estimate at each time step.

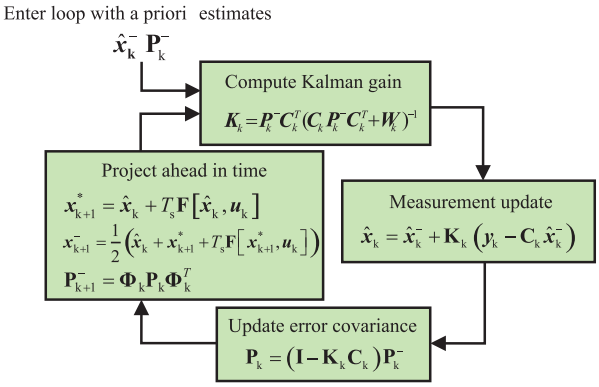

Fig. 2: *Extended Kalman Filter loop*

4 Experiment and Simulation Setup

Figure 3 shows the actual construction of the metering poppet valve system set up in the lab to run the test. An amplifier (controlled by a signal from a computer which is also used to gather sensor data) was used to supply current to the valve actuator solenoid. The current was measured using a current sensor which was placed in the electrical circuit between the amplifier and solenoid. A known relationship between current and force was used so that the force input to the system could be determined as needed.

A dither signal was applied to the valve solenoid current commands to reduce nonlinear friction effects. The dither signal frequency and amplitude were 100 Hz and 120 mA. The dither signal had a small influence on the position of the main poppet (other than eliminating static friction effects). In particular, it could be seen from experimental results that a low amplitude 100 Hz component was superimposed on the position response. The benefit of the dither signal was that the sticking friction of the valve was significantly reduced. Prior to adding dither, simulation and experimental responses did not compare well due to a lack of a nonlinear friction model. After adding dither, the simulations and experimental results matched well.

A pressure supply was connected to the inlet port of the valve. The outlet port was connected to a line leading to the hydraulic reservoir as shown in Fig 3. Pressure sensors were placed near the inlet and outlet ports to measure P_S and P_L. Another pressure sensor was installed to measure P_C in order to compare the result simulated from the model and the result estimated from the EKF and to supply the measured output signal that was used in the EKF. An LVDT sensor was attached to the main poppet during the test for measuring main poppet position for the purpose of comparing to estimated and simulated results as well.

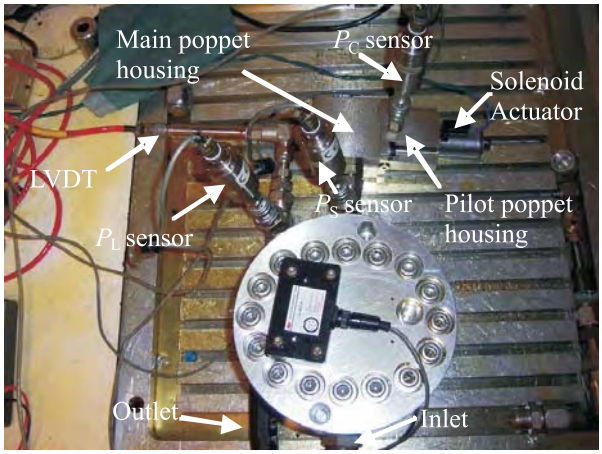

Fig. 3: *Metering poppet valve system*

The EKF estimator was examined by constructing MATLAB and SIMULINK models for both the valve system and the EKF estimator. Modifications were made to the system model used in the EKF in order to allow the EKF to operate with accuracy when the experimental conditions are such that the actual poppet positions and pressures are at their physical limits. The EKF was improved by adding limits to the algorithm. For the main and pilot poppets, if the estimated position of the poppet exceeds the upper limit or the lower limit, it is correspondingly set to the maximum displacement, x_{max}, or the minimum displacement, x_{min}. Simultaneously the estimated velocity of the poppet is set to zero. Also, the estimated acceleration of the poppet is determined by both the position and acceleration. If the poppet hits a limit and the acceleration of the poppet shows it is moving outside the limits, the acceleration is then set to zero. Whenever the estimated values for P_C and P_P exceed the maximum pressure limit, P_{max}, they are reset to the maximum pressure. The maximum pressure limit is the same as the relief valve setting in the lab. When the pressures are below the minimum pressure setting, P_{min}, they are reset to the minimum pressure, zero gage pressure. The partial derivatives used in the state transition matrix are calculated based on the states after the limitations are applied. Therefore, whenever the actual states hit their physical limits, the EKF can also estimate states properly at these limits. To apply the limitations, the values of x, $\dot{x}$, $\ddot{x}$, and P_C will be modified according to the equations in Table 1. (Note that the limits on y are similar to x and the limits on P_P are similar to P_C)

In the actual simulation, the sampling time, T_s, is set to 10^{-5} s in order to track the fast response during tran-

sient periods. When the pressure measurement for P_C is around 10^7 Pa, the measurement noise from the pressure sensor is around 10^5 Pa, which means the sensor has a relative measurement accuracy of 1 %. Many pressure sensors meet this specification. Therefore the measurement noise variance is set to be $(10^5\ \text{Pa})^2$, which indicates the EKF can work by using low accuracy pressure sensor measurements. Therefore,

$$\mathbf{W}_k = [(10^5\ \text{Pa})^2] \tag{19}$$

Table 1: Limitations applied to estimated states

$x = \begin{cases} x_{min} & if\ x \le x_{min} \\ x & if\ x_{min} < x < x_{max} \\ x_{max} & if\ x \ge x_{max} \end{cases}$	$\dot{x} = \begin{cases} 0 & if\ x \le x_{min} \\ \dot{x} & if\ x_{min} < x < x_{max} \\ 0 & if\ x \ge x_{max} \end{cases}$
$\ddot{x} = \begin{cases} 0 & if\ x \le x_{min}\ \&\ \ddot{x} < 0 \\ \ddot{x} & if\ x \le x_{min}\ \&\ \ddot{x} > 0 \\ \ddot{x} & if\ x_{min} < x < x_{max} \\ \ddot{x} & if\ x \ge x_{max}\ \&\ \ddot{x} < 0 \\ 0 & if\ x \ge x_{max}\ \&\ \ddot{x} > 0 \end{cases}$	$P_C = \begin{cases} P_{min} & if\ P_C \le P_{min} \\ P_C & if\ P_{min} < P_C < P_{max} \\ P_{max} & if\ P_C \ge P_{max} \end{cases}$

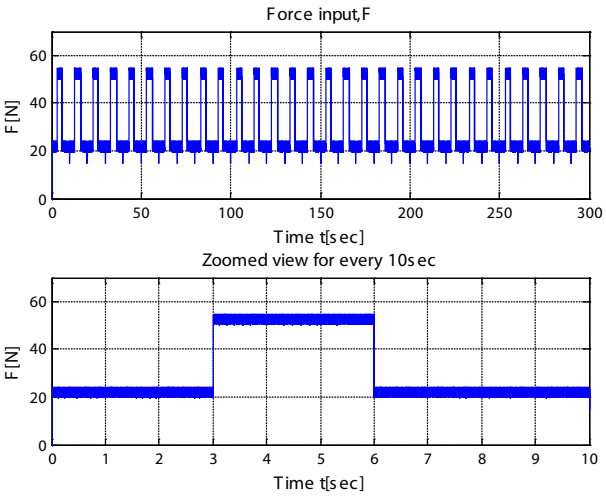

Fig. 4: *Force input*

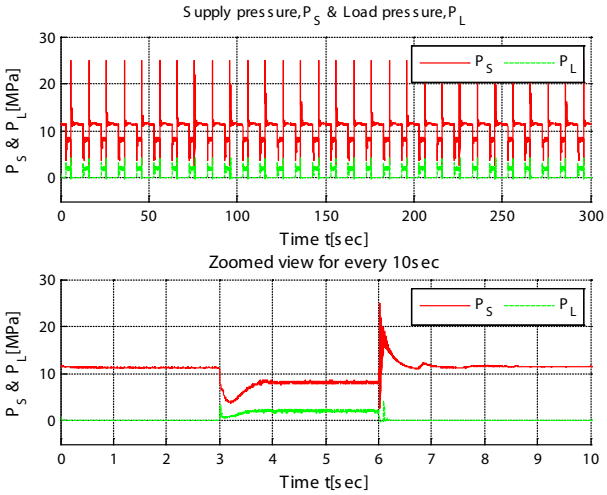

Fig. 5: *Supply pressure and load pressure*

In order to observe the workability and drifts in the estimation of the EKF in a long test run, the EKF is run for 5 minutes. Therefore a repeated square wave force generated by the solenoid, shown in Fig. 4, is applied to the actual metering poppet valve system and the measured force is applied to the system model and EKF as the only input. The supply pressure, P_S, and load pressure, P_L, shown in Fig. 5, are measured and applied to the system model and EKF as parameters. Therefore the physical system, system model and EKF are run under the same conditions. The output of the system, P_C, is measured and used in the EKF for estimating all the states of the valve.

The initial guess of the state vector, $\hat{\boldsymbol{x}}^-$, is set to $[0\ 0\ 0\ 0\ 0\ 0]^T$. The initial guess of the error covariance matrix, $\mathbf{P}^-$, which is shown in part II of the Appendix, is carefully selected to get the filter to converge and yield good estimator performance. The error covariance matrix initial guess was chosen by trial and error. Small values in $\mathbf{P}^-$ caused the EKF to produce noisy estimates while larger values yielded less noise.

5 Experimental Results

Figures 6 through 9 show the performance of the Extended Kalman Filter for estimating the positions and velocities of the pilot and main poppets during the transients and steady state portions of the experiment. The four estimated states from EKF match the simulated states from the model well. Periodically the input force changes from 22 N to 53 N and after 3 seconds the input force drops back to 22 N. It takes less than 0.05 sec for the EKF estimator to track the position and velocity of both the pilot and main poppets. The dynamics of the pilot poppet velocity and main poppet velocity are very fast, however the estimated states from the EKF closely resemble the results from the simulation and have almost no delay.

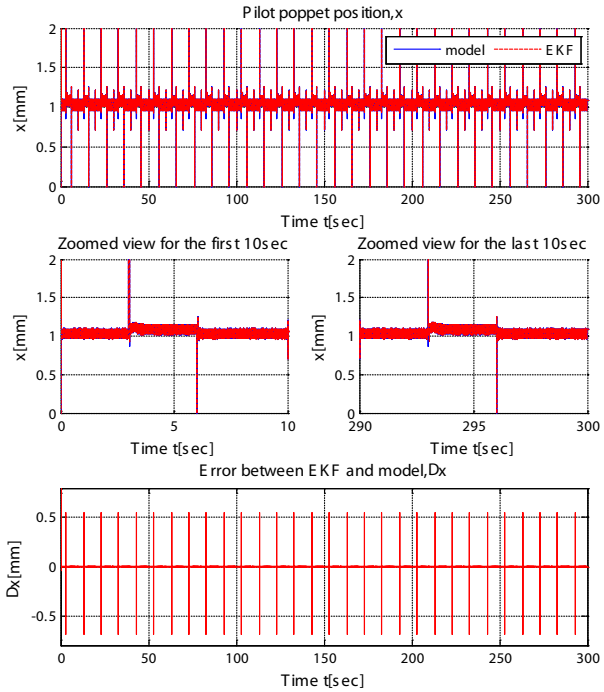

Fig. 6: *Estimation of pilot poppet position*

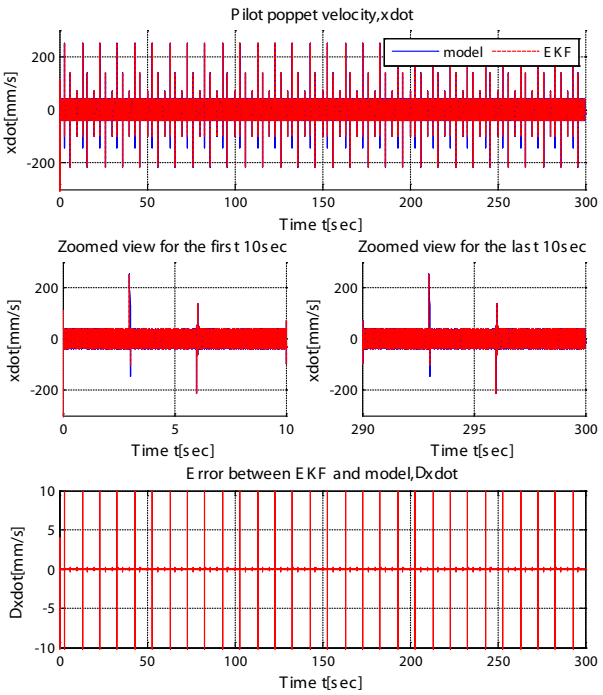

Fig. 7: *Estimation of pilot poppet velocity*

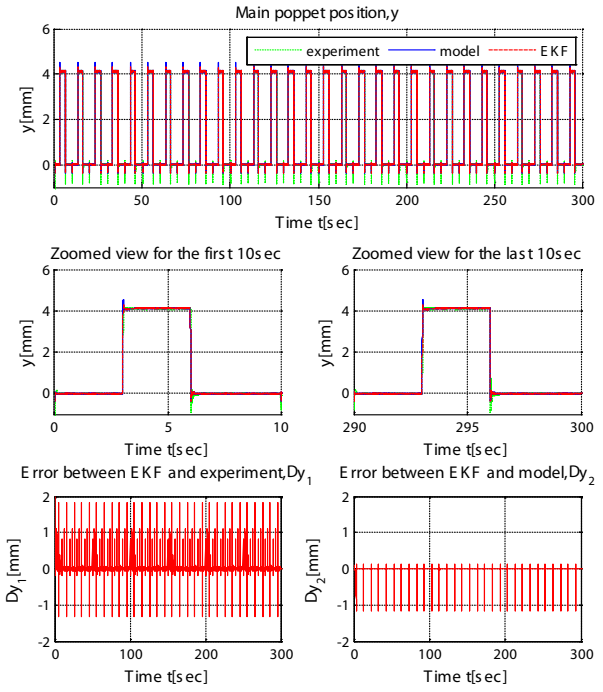

Fig. 8: *Estimation of main poppet position*

The main poppet position is also measured by an LVDT from the actual system in order to check the results from the EKF. In Fig. 8, the error between the estimated main poppet position from EKF and the measured value from the LVDT also remains near zero except for some small oscillations during the transient period, but they all decay very quickly.

Figure 8 also shows that when the main poppet position is zero the estimation from EKF is zero also which indicates the algorithm for setting limits added in the EKF program works well in the simulation.

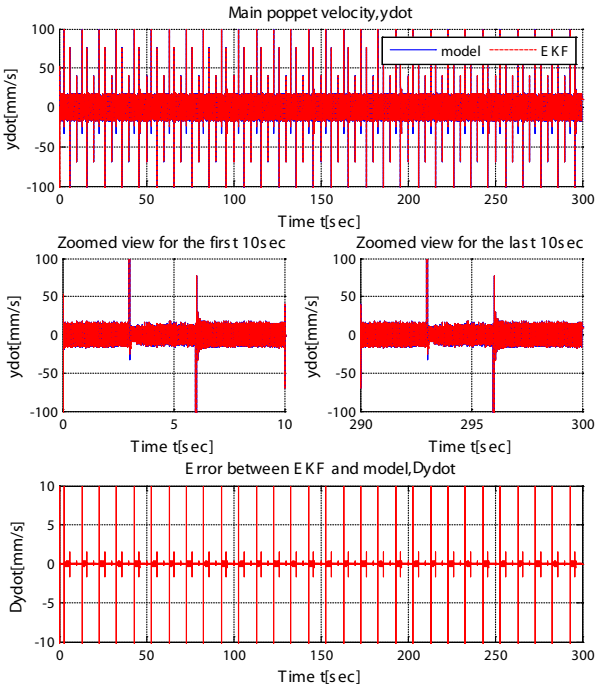

Fig. 9: *Estimation of main poppet velocity*

In Fig. 6 through 9, the errors between estimated states from EKF and states simulated from the model remain near zero during the entire operation. There are some oscillations when the force input steps up and down, but these oscillations decay away extremely quickly and all the relative errors are less than 10%, which is within the requirement.

From the zoomed view for the first 10 seconds and last 10 seconds in Fig. 6 through 9, it is clear that the four states do not have significant drift and converge from the beginning to the end during the whole simulation.

Figure 10 and Fig. 11 show the estimations for the two pressures, P_C and P_P.

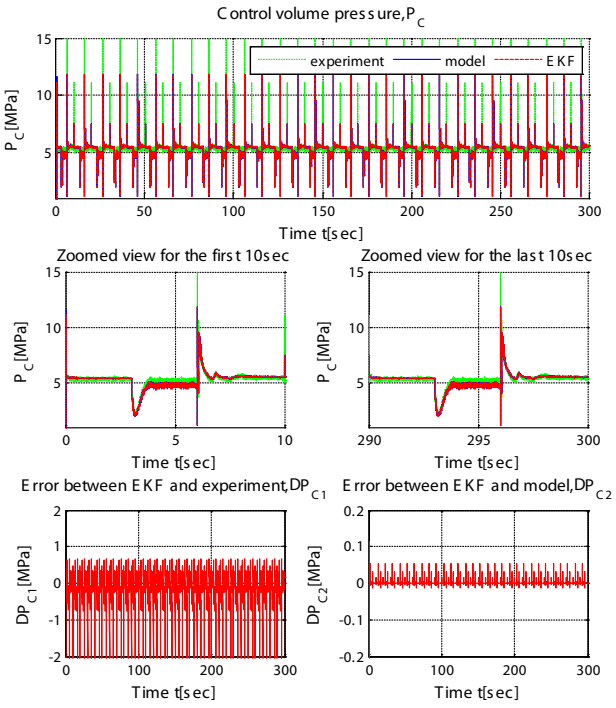

Fig. 10: *Estimation of control volume pressure*

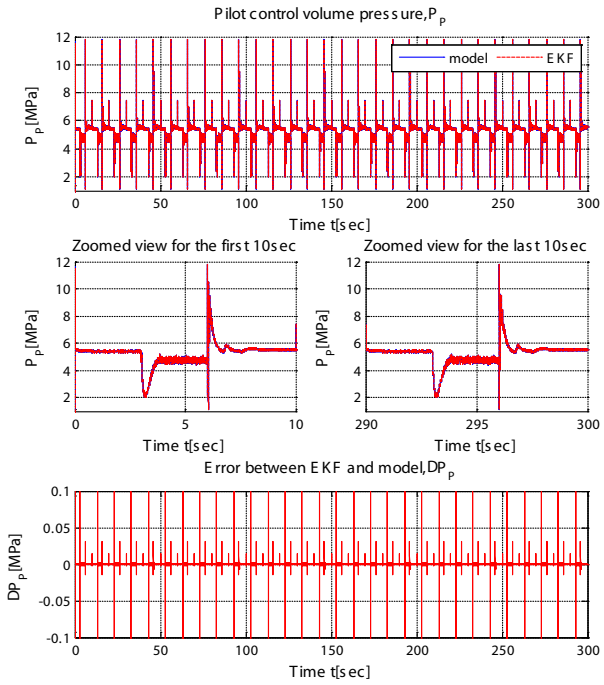

Fig. 11: *Estimation of pilot control volume pressure*

In Fig. 10 and Fig. 11 the oscillations in the error between EKF and model simulation caused by the force input change return to zero very quickly and stay around zero at other times during the simulation. Figure 10 also shows the measurement for P_C from the sensor. The error between the measured value and the estimated value is always near zero except for some small variation which is within acceptable limits.

The zoomed view for the first 10 seconds and last 10 seconds in Fig. 10 and 11 also show that the estimation for P_C and P_P do not have any drift and converge during the entire simulation. Combined with the zoomed view in Fig. 6 through Fig. 9, all these plots show that the EKF can be used in a long run.

6 Robustness

In order to check the robustness of the Extended Kalman Filter, a test is carried out by giving the EKF a wrong piece of information relating to a parameter. The spring rate in the system has an important effect on the dynamics of the system and it is also hard to manufacture precisely. Therefore, the spring rate, k, is chosen as a parameter to be changed for test. The spring rate is increased by 10 % for the EKF while the experimental setup and simulation are left unchanged. For the case where the EKF is designed with this incorrect value of k, the corresponding max relative errors for the estimates are compared with the max relative errors for the estimates using the original spring rate as shown in Table 2. For the main poppet position, y, and control volume pressure, P_C, the EKF estimates are compared with the experiment data. The EKF estimates of the other states shown in Table 2 are compared with the model simulation since these states can not be measured.

Table 2: Comparison for max relative error

States	Max relative error for original spring rate	Max relative error for modified spring rate
x	0.0183 %	0.43 %
$\dot{x}$	0.32 %	2.5 %
y	0.49 %	8.78 %
$\dot{y}$	3.33 %	5 %
P_C	7.69 %	9.67 %
P_P	0.0421 %	0.38 %

With the increase of the spring rate, the maximum relative errors of all the states are increased. The max relative error of the main poppet position, y, has the largest increase because the spring has direct impact on the main poppet. But all the max relative errors with the modified spring rate for all the states are less than 10%, which is still within the requirement. This indicates that the EKF has robustness to the spring rate variation.

7 Conclusion

In this paper, the application of Extended Kalman Filter in the Forced-Feedback Metering Poppet Valve System, which is a nonlinear, dynamic system, is discussed. Fortunately, for this particular system at a linearized operating point, the system is observable and the EKF is stable for all operating conditions tested in the lab. Therefore the performance of the EKF is satisfactory during operation. When the input changes, the estimated states from the EKF follow closely to the true states for both the steady and transient portions of the experiments. This indicates the tractability of the EKF estimator. When model uncertainty appears in the EKF in the form of an uncertain feedback spring constant, the max errors of the estimated states are within the reasonable limit of 10 %. This supports the claim that the EKF estimator is robust to parameter variation.

Future work will focus on the implementation of a PID or H_∞ controller to the system using the estimated states from the Extended Kalman Filter. Further studies are also needed to conclusively prove that the EKF is robust to a wide variety of parameter variations such as changes in friction due to contamination etc. While the dither signal discussed in Section 4 reduced the effects of nonlinear friction, the inclusion of a nonlinear friction model and experimental verification is also a subject of further study to help improve the accuracy of the model.

Nomenclature

a_{1max}	area of variable inlet orifice when poppet is closed	[m^2]
A_C	area of main poppet exposed to control pressure	[m^2]
A_L	area of main poppet exposed to load pressure	[m^2]
A_{pilot}	area of pilot poppet exposed to pilot pressure	[m^2]
A_{pist}	area of load piston exposed to load pressure	[m^2]
A_S	area of main poppet exposed to supply pressure	[m^2]
b_x	linear pilot poppet damping	[Ns/m]
b_y	main poppet damping	[Ns/m]
b_z	load piston damping	[Ns/m]
F_{load}	working load force on the load piston	[N]
h_1	area gradient to control volume inlet orifice	[m]
h_2	area gradient to control volume outlet orifice	[m]
h_3	area gradient to main poppet orifice	[m]
L_{pilot}	pilot tube length	[m]
k	feedback spring coefficient	[N/m]
m	mass of the pilot poppet	[kg]
M	mass of the main poppet	[kg]
M_{pist}	mass of the load piston	[kg]
preload	initial displacement of the feedback spring	[m]
R	radius of pilot tube	[m]
V_C0	fluid volume between main poppet and pilot poppet when closed	[m^3]
V_{load}	fluid volume between the valve and the retracted load piston	[m^3]
$V_{pilot}0$	fluid volume between closed pilot poppet and solenoid housing	[m^3]
C_d	orifice discharge coefficient	
β	fluid bulk modulus	[Pa]
ρ	fluid density	[kg/ m^3]
μ	fluid viscosity	[Ns/ m^2]
θ	jet angle for flow force	
x	pilot poppet position	[m]
$\dot{x}$	pilot poppet velocity	[m/s]
$\ddot{x}$	pilot poppet acceleration	[m/s^2]
y	main poppet position	[m]
$\dot{y}$	main poppet velocity	[m/s]
$\ddot{y}$	main poppet acceleration	[m/s^2]
P_C	control volume pressure between the main poppet and pilot poppet	[Pa]
P_P	control volume pressure between the pilot poppet and the actuator housing	[Pa]
P_S	supply pressure	[Pa]
P_L	return line pressure	[Pa]
f_1	flow force on pilot poppet	[N]
f_2	flow force on pilot poppet	[N]
f_3	flow force on main poppet	[N]
F	actuator force on the pilot poppet	[N]
Q_1	flow rate across the inlet orifice to control volume	[m^3/s]
Q_2	flow rate across the outlet orifice from control volume	[m^3/s]
Q_6	low Re tube flow through a circular tube in the pilot poppet	[m^3/s]

Acknowledgments

The authors would like to thank Matthew Muller and Mike Knussman for their helpful suggestions and discussion.

Reference

Acarnley, P. P. and **AI-Tayie, J. K.** 1997. Estimation of speed and armature temperature in a brushed DC drive using the extended Kalman filter. *Electric Power Application, IEE Proceedings,* Vol. 144, Issue 1, pp. 13-20.

An, L. and **Sepehri, N.** 2005. Hydraulic Actuator Leakage Fault Detection Using Extended Kalman Filter. *International Journal of Fluid Power,* Vol. 6, pp. 41-51.

Chinniah, Y., **Burton, R.** and **Habibi, S.** 2003. Viscous Damping Coefficient and Effective Bulk Modulus Estimation in a High Performance Hydrostatic Actuation System using Extended Kalman Filter. *International Journal of Fluid Power*, Vol. 4, No. 3, pp. 27-34.

Fales, R. and **Li, C.** 2008. Experimental Evaluation of a Metering Poppet Valve. *Bath/ASME Symposium on Fluid Power & Motion Control*, Bath, UK.

Manring, N. D. 2005. *Hydraulic Control Systems.* John Wiley and Sons, New Jersey, pp. 224-228.

Muller, M. and **Fales, R.** 2008. Design and Analysis of a Two-Stage Poppet Valve for Flow Control. *International Journal of Fluid Power*, Vol. 9, No. 1, pp. 17-26.

Walchko, K. J., **Novick, D.** and **Nechyba, M. C.** 2003. Development of a Sliding Mode Control System with Extended Kalman Filter Estimation for Subjugator. *Florida Conference on Recent Advances in Robotics*, FAU, Dania Beach, FL.

Zhuang Xu. and **Rahman, M. F.** 2003. An Extended Kalman Filter Observer for the Direct Torques Controlled Interior Permanent Magnet Synchronous Motor Drive. *Power Electronics and Drive Systems,* The Fifth International Conference. Vol. 1, pp. 686-691.

Appendix

I. Detailed Calculation of the Elements of the State Space Matrix:

$$f_{21}=\frac{-k+2\cos(\theta)C_d^2h_1(P_S-P_C)-2\cos(\theta)C_d^2h_2(P_C-P_L)}{m}$$

$$f_{22}=-\frac{b_x}{m}\quad f_{23}=-\frac{k}{m}$$

$$f_{25}=-\frac{A_{pilot}+2\cos(\theta)C_d^2(h_1x+a_{1max})+2\cos(\theta)C_d^2h_2x}{m}$$

$$f_{26}=\frac{A_{pilot}}{m}\quad f_{41}=-\frac{k}{m}\quad f_{43}=-\frac{k+2\cos(\theta)C_d^2h_3(P_S-P_L)}{M}$$

$$f_{44}=-\frac{b_y}{M}\quad f_{45}=-\frac{A_C}{M}$$

$$f_{51}=\beta\frac{(V_C0-A_{pilot}x-A_Cy)\left(\frac{\partial Q_1}{\partial x}-\frac{\partial Q_2}{\partial x}\right)+A_{pilot}(Q_1-Q_2-Q_6+A_C\dot{y})}{(V_C0-A_{pilot}x-A_Cy)^2}$$

$$f_{53}=\frac{\beta A_C(Q_1-Q_2-Q_6+A_C\dot{y})}{(V_C0-A_{pilot}x-A_Cy)^2}\quad f_{54}=\frac{\beta A_C}{V_C0-A_{pilot}x-A_Cy}$$

$$f_{55}=\beta\frac{\frac{\partial Q_1}{\partial P_C}-\frac{\partial Q_2}{\partial P_C}-\frac{\partial Q_6}{\partial P_C}}{V_C0-A_{pilot}x-A_Cy}\quad f_{56}=-\frac{\beta\frac{\partial Q_6}{\partial P_P}}{V_C0-A_{pilot}x-A_Cy}$$

$$f_{61}=-\frac{\beta A_{pilot}(Q_6-A_{pilot}\dot{x})}{(V_{pilot}0+A_{pilot}x)^2}\quad f_{62}=-\frac{\beta A_{pilot}}{V_{pilot}0+A_{pilot}x}$$

$$f_{65}=\frac{\beta\frac{\partial Q_6}{\partial P_C}}{V_{pilot}0+A_{pilot}x}\quad f_{66}=\frac{\beta\frac{\partial Q_6}{\partial P_P}}{V_{pilot}0+A_{pilot}x}$$

where

$$\frac{\partial Q_1}{\partial x}=C_dh_1\sqrt{\tfrac{2}{\rho}(P_S-P_C)}\quad \frac{\partial Q_1}{\partial P_C}=-\frac{C_d(h_1x+a_{1max})}{\sqrt{2\rho(P_S-P_C)}}$$

$$\frac{\partial Q_2}{\partial x}=C_dh_2\sqrt{\tfrac{2}{\rho}(P_C-P_L)}\quad \frac{\partial Q_2}{\partial P_C}=\frac{C_dh_2x}{\sqrt{2\rho(P_C-P_L)}}$$

$$\frac{\partial Q_6}{\partial P_C}=\frac{\pi R^4}{8\mu L_{pilot}}\quad \frac{\partial Q_6}{\partial P_P}=-\frac{\pi R^4}{8\mu L_{pilot}}$$

II. Initial Guess of the Error Covariance Matrix:

$$\mathbf{P}^-=\begin{bmatrix}10^7&0&0&0&0&0\\0&10^7&0&0&0&0\\0&0&10^7&0&0&0\\0&0&0&10^7&0&0\\0&0&0&0&10^7&0\\0&0&0&0&0&10^7\end{bmatrix}$$

Chang Li
Received a B.S in Measurement, Control Technology and Instruments from Shanghai Jiao Tong University in 2004. Candidate for Ph.D in Department of Mechanical and Aerospace Engineering in University of Missouri-Columbia from 2006. His research focuses on system design, analysis and control related area.

Roger Fales
Fales received B.S. and M.S. degrees in Mechanical Engineering at Kansas State University in 1996 and 1998 respectively. He was employed at Caterpillar Inc. from 1998 to 2002 as a research engineer. At Iowa State University, he received a Ph.D. in Mechanical Engineering in 2004. In 2004, he joined the Mechanical & Aerospace Engineering Department at the University of Missouri – Columbia. As an assistant professor, he teaches and does research work in the areas of dynamics, systems, automatic control, and fluid power.